

Published in final edited form as:

*Nat Chem Biol.* 2017 January ; 13(1): 21–29. doi:10.1038/nchembio.2217.

## Structure of p300 in complex with acyl-CoA variants

Zuzanna Kaczmarek<sup>#1</sup>, Esther Ortega<sup>#1</sup>, Afsaneh Goudarzi<sup>2</sup>, He Huang<sup>3</sup>, Sunjoo Kim<sup>3</sup>, José A Márquez<sup>1</sup>, Yingming Zhao<sup>3</sup>, Saadi Khochbin<sup>2</sup>, and Daniel Panne<sup>1,\*</sup>

<sup>1</sup>European Molecular Biology Laboratory, Grenoble, France

<sup>2</sup>Université Grenoble Alpes, Institut Albert Bonniot, Grenoble, France

<sup>3</sup>Ben May Department of Cancer Research, The University of Chicago, Chicago, Illinois, USA

# These authors contributed equally to this work.

### Abstract

Histone acetylation plays an important role in transcriptional activation. Histones are also modified by chemically diverse acylations that are frequently deposited by p300, a transcriptional coactivator that uses a number of different acyl-CoA cofactors. Here we report that while p300 is a robust acetylase, its activity gets weaker with increasing acyl-CoA chain length. Crystal structures of p300 in complex with propionyl-, crotonyl-, or butyryl-CoA show that the aliphatic portions of these cofactors are bound in the lysine substrate-binding tunnel in a conformation that is incompatible with substrate transfer. Lysine substrate binding is predicted to remodel the acyl-CoA ligands into a conformation compatible with acyl-chain transfer. This remodeling requires that the aliphatic portion of acyl-CoA be accommodated in a hydrophobic pocket in the enzymes active site. The size of the pocket and its aliphatic nature exclude long-chain and charged acyl-CoA variants, presumably explaining the cofactor preference for p300.

Spatial and temporal regulation of chromatin is an important aspect of all DNA-templated processes in eukaryotic cells, including gene transcription, DNA replication and DNA repair. Chromatin function is regulated at several levels, including incorporation of histone variants, remodeling by ATP-dependent remodeling enzymes and post-translational modification (PTM) of histones. Enzymes that catalyze histone PTMs frequently use cofactors that are derived from primary metabolism, providing a link between the metabolic state of the cell and gene regulation<sup>1</sup>. For example, chromatin acetylation, a modification usually associated

\*Correspondence and requests for materials should be addressed to D.P. panne@embl.fr.

#### Author contributions

Z.K. performed the structure determination of p300 under supervision of J.A.M. and D.P. E.O. and Z.K. performed biochemical assays. E.O. prepared the constructs and performed protein expression and purification. A.G. performed the IP-HAT experiments under the supervision of S. Khochbin. H.H. and S. Kim performed MS experiments under the supervision of Y.Z. D.P. designed and coordinated the project, advised and assisted on all aspects of the project and wrote the manuscript. All authors discussed the results and commented on the manuscript.

#### Competing financial interests

The authors declare no competing financial interests.

#### Additional information

Reprints and permissions information is available online at <http://www.nature.com/reprints/index.html>.

**Accession codes.** Atomic coordinates and structure factors of the reported crystal structure have been deposited in the Protein Data Bank under the accession codes: [5LKU](#) (endogenous CoA); [5LKT](#) (butyryl-CoA); [5LKZ](#) (crotonyl-CoA); [5LKX](#) (propionyl-CoA).

with active gene transcription, is catalyzed by acetyltransferases (HATs), enzymes that transfer an acetyl group from the metabolite acetyl-CoA to the  $\epsilon$ -amino group of lysine<sup>2</sup>. Lysine acetylation provides binding sites for effector proteins containing bromodomains, domains that are prevalent in nuclear proteins that interact with chromatin<sup>3</sup>. Histone deacetylases (HDACs) remove such chromatin modifications, and the combined actions of writing, reading and erasure of histone acetylation, and histone modifications in general, provide a mechanism for differential regulation of chromatin function and gene expression<sup>4</sup>.

In addition to acetylation, histone lysine residues can also be modified by chemically diverse acyl modifications, including formylation, propionylation, butyrylation, 2-hydroxyisobutyrylation,  $\beta$ -hydroxybutyrylation, crotonylation, malonylation, succinylation, glutarylation, 4-pentynoylation, 3-phosphoglyceroylation, palmitoylation and myristoylation<sup>5–15</sup>. These modifications are derived from their respective charged acyl-CoAs, small-molecule intermediates derived from pathways of cellular energy metabolism. As the concentrations of various acyl-CoAs fluctuate as a function of the metabolic state of the cell, metabolism potentially directly influences cellular signaling and transcriptional activation by modulating differential protein and histone acylation<sup>5,6,9,16,17</sup>.

The identification of various histone lysine acylations raises the questions of which enzymes mediate their deposition, how they are removed, and whether there are binding domains that recognize such modifications. A recent investigation of the capacity of human bromodomains to bind acyllysine modifications revealed that while most bromodomains analyzed are able to bind to acetyl- and propionyllysine, most do not bind the longer butyryl- or crotonyllysine modifications<sup>18</sup>. Thus, the longer acylations can potentially inhibit binding of bromodomain proteins, as was shown recently for histone H4K5 butyrylation, which prevents binding of Brdt, with the result that histone removal is delayed in spermatogenic cells<sup>19</sup>. Recent data also support the notion that there are specialized ‘reader’ domains, such as the YEATS domain, that preferentially recognize the crotonyllysine modification<sup>20,21</sup>.

Removal of long-chain lysine acylations is mediated by several HDACs. SIRT5 preferentially removes acidic acyl modifications such as malonyl<sup>12,22</sup>, succinyl<sup>12,22,23</sup> or glutaryl<sup>10</sup>. Short-chain fatty acyl modifications such as propionyl, butyryl or crotonyl are removed by several sirtuins<sup>24–28</sup>, while long-chain fatty acyl modifications can be removed by SIRT6 (refs. 25,29).

How enzymes catalyze diverse lysine acylations is less well understood. Based on the sequence divergence, HATs have been grouped into at least five different families<sup>30</sup>. Three HAT family members have been reported to catalyze short-chain lysine acylation *in vitro*. p300–CREB binding protein (CBP) (KAT3B and KAT3A nomenclature according to ref. 31) catalyze propionylation, crotonylation and butyrylation on chromatin, p53 and p300 itself<sup>5,24,32</sup>. p300-mediated crotonylation also occurs in cells, and crotonylation levels are directly regulated by the cellular concentration of crotonyl-CoA<sup>32</sup>. Like acetylation, crotonylation and butyrylation by p300 also stimulate gene transcriptional activity in cell-free assays<sup>19,32</sup>. Some data also suggest that p300 can catalyze acidic acyllysine modifications including glutarylation and succinylation<sup>10,33</sup>. Other HATs such as P300–CBP-associated factor (PCAF) and human GCN5 (hGCN5) catalyze propionylation of a

histone H3 peptide, and yeast Esa1, a MYST family member, catalyzes propionylation of a histone H4 peptide<sup>34</sup>. The activity of PCAF gets weaker with increasing acyl-chain length<sup>35</sup>. Recently it was shown that the deletion of *hat1*, *gcn5* and *rtt109* in yeast leads to a considerable reduction of histone H3 Lys9 (H3K9) crotonylation *in vivo*, with the most dramatic effects observed upon *gcn5* deletion, suggesting that this modification is incorporated by yeast GCN5 (yGCN5)<sup>20</sup>. Structural and biochemical data show, however, that hGCN5 cannot hydrolyze longer acyl-CoA variants<sup>36</sup>. While the active site of hGCN5 can bind propionyl-CoA and butyryl-CoA, the latter adopts a conformation that does not allow catalysis to occur, indicating that the longer acyl-chain variants act as competitive inhibitors for hGCN5 (ref. 36). Other HATs such as hMOF and hTIP60 also appear to not use the longer crotonyl-CoA as substrate<sup>32</sup>. Thus, while most HATs are more restrictive with regards to acyl-chain length, p300 can utilize a chemically diverse set of acyl-CoA cofactors.

To start to address how p300 can accommodate chemically and sterically diverse acyl-CoA cofactors in the active site in a conformation that is compatible with the binding of protein substrates and transfer of the acyl moiety, we have systematically analyzed p300-mediated histone H3–H4 acylation. In agreement with previously published data, we found that short-chain acyl-CoA variants can be used as p300 substrates, but that the acyltransferase activity gets weaker with increasing acyl-chain length. X-ray crystal structures of the p300 core in complex with propionyl-, crotonyl-, and butyryl-CoA revealed that the active site of p300 accommodates longer acyl chains without major structural rearrangements. The aliphatic portions of the acyl-CoA variants are positioned in the lysine substrate-binding tunnel and would sterically clash with the incoming substrate. We propose that substrate engagement results in remodeling of the short chain acyl-CoA ligands into a conformation compatible with acyl-chain transfer. We identify a hydrophobic pocket in the enzyme's active site that is predicted to accommodate the aliphatic portion of the remodeled acyl-CoA. The size of the pocket and its aliphatic nature apparently restrict against long-chain and charged acyl-CoA variants, presumably explaining the cofactor preference for p300. The lack of such a pocket in other HATs such as hGCN5, TIP60 and MOF explains the more restricted acyl-CoA cofactor requirement for these acetyltransferases.

## Results

### p300 can use a diverse array of acyl-CoAs as substrates

p300 activation is accompanied by trans-autoacetylation in a lysine-rich autoinhibitory loop (AIL) spanning residues 1520–1581 that is embedded in the HAT domain<sup>37</sup>. To assess which acyl-CoA variants are compatible with p300 autoacetylation, we used a *trans*-autoacetylation assay in which one catalytically deficient p300 variant (p300\_core) is acylated by a wild-type version of the enzyme (p300s) and monitored the reaction by LC–MS (Fig. 1a–c). The p300\_core variant used in these experiments contained an inactivating mutation of the catalytic Tyr residue (Y1467F), which reduces, but does not completely abolish, p300 activity<sup>38</sup>. Accordingly, insect-cell-purified p300\_core showed a series of peaks (+42 Da) corresponding to autoacetylation of the enzyme (Fig. 1a). Upon incubation with p300s, we observed a series of +42 Da adducts corresponding to acetylated p300,

presumably located in the lysine-rich AIL. Similarly, we observed a series of adducts upon addition of butyryl-CoA or propionyl-CoA, indicating that these acyl-CoA variants can be used by p300 in a *trans*-autoacylation reaction (Fig. 1b,c). Because of the high reactivity of these acyl-thiol compounds, it is important to distinguish between enzyme-catalyzed and non-enzymatic acylation. As we only observed an increase in p300\_core acylation in the presence of p300s but not when incubated only with acyl-CoA, we conclude that p300 can use these acyl-CoAs as acylation donors (Fig. 1a–c).

Next, we investigated whether p300 can also incorporate these acylations into protein substrates. We incubated p300s with *Xenopus laevis* histones H3 and H4 that had been recombinantly produced in *Escherichia coli*, and allowed to re-fold to form H3–H4 tetramers, and then we analyzed the reaction products by LC–MS. These *Xenopus* histones were already partially acetylated before incubation with p300s (Fig. 1d). In the presence of acetyl-CoA we observed significantly increased acetylation (Fig. 1d). In the presence of butyryl- or propionyl-CoA, we observed additional mass peaks that corresponded to the respective acyl-CoA variant used (Fig. 1e,f); however, we observed fewer modified peaks than for the acetyl-CoA treated sample, indicating that the activity of p300 gets weaker with increasing acyl-chain length. We also analyzed histone acylations using a western blot. We found that p300 also supported crotonylation and  $\beta$ -hydroxybutyrylation, a modification shown recently to occur in chromatin<sup>14</sup>, but incubation with 2-hydroxyisobutyryl-CoA resulted in non-enzymatic acylation, presumably because of the high reactivity of this acyl-CoA variant (Supplementary Results, Supplementary Fig. 1a,b).

To further analyze the observed decrease in catalytic efficiency, we compared the catalytic rates of hydrolysis of the acyl-CoA variants by p300 in the presence of a histone H3 peptide. We found that while p300 efficiently hydrolyzed acetyl- and propionyl-CoA, its butyrylation and crotonylation activities were less efficient (Fig. 1g). p300 propionylated the H3 peptide approximately three-fold more slowly, while it butyrylated and crotonylated about 40-fold and nearly 62-fold more slowly, respectively, as compared to its acetyltransferase activity (Fig. 1g). Thus, we observed a direct correlation between the length of the acyl-CoA chain and the efficiency of hydrolysis, with the longer variants being less-efficiently hydrolyzed by p300.

### Structure determination of acyl-CoA-bound p300

To elucidate the structural basis for the acyl-CoA chain preference of p300, we determined the structures of p300 bound to propionyl-, crotonyl- and butyryl-CoA. Previous structural studies of the catalytic 'core' required introduction of the inactivating Y1467F mutation and deletion of the flexible AIL that harbors multiple lysine acetylation sites (p300\_core ; Supplementary Fig. 1c)<sup>39</sup>. Expression of p300\_core in insect cells results in residual autoacetylation, and successful crystallization previously required further deacetylation with SIRT2 (ref. 39). To facilitate structural studies we have established a coexpression system for p300\_core and SIRT2. Coexpression in insect cells allowed expression of high yields of p300\_core (Supplementary Fig. 2a), and size-exclusion chromatography showed that such preparations are homogeneous (Supplementary Fig. 2b). MS analysis showed that p300\_core purified in the absence of SIRT2 is autoacetylated, as revealed by a series of

peaks shifted by  $\sim +42$  Da relative to the unacetylated p300\_core (Supplementary Fig. 2c). Upon coexpression of SIRT2, mostly the deacetylated form was obtained (Supplementary Fig. 2c). Thus, p300 preferentially uses endogenous acetyl-CoA, but not other acyl-CoA variants, at least under the fermentation conditions used upon overexpression in insect cells. This modified purification procedure allowed us to crystallize the p300\_core bound to various ligands without the additional deacetylation step that was previously required<sup>39</sup>. All crystal structures were determined by molecular replacement using the p300 core structure (PDB code 4BHW) with the lysyl-CoA ligand omitted from the search model. Data collection and refinement statistics for all structures are listed in Supplementary Table 1.

### Structure of p300 bound to various acyl-CoA ligands

The overall structure of p300 in complex with the different CoA ligands is essentially identical to that seen in the p300-lysyl-CoA complex<sup>39</sup>. The structure encompasses the bromodomain, the CH2 region containing a PHD domain that is interrupted by a RING domain, and the HAT domain (Fig. 2a). The bromodomain, PHD, RING and HAT domains adopt an assembled configuration in which the RING domain is juxtaposed to the HAT substrate-binding site. The CoA binding pocket in the butyryl-CoA liganded structure has the same architecture as that in the lysyl-CoA structure (Fig. 2b). The substrate-binding loop between  $\alpha 4$  and  $\beta 5$  encapsulates the CoA ligand: Arg1462 and Lys1456 sandwich the adenosine ring, Arg1410 makes several critical hydrogen bonds to phosphates, and the pantetheine arm of CoA makes extensive interactions with the substrate-binding loop (Fig. 2b).

The structures obtained with the lysyl-CoA bisubstrate inhibitor mimic a post-reaction CoA-lysine intermediate, while the structures of the isolated HAT domain in complex with acetyl-CoA and CoA represent pre- and post-reaction conformations, respectively<sup>38–40</sup>. We were able to crystallize p300\_core in the absence of extraneously added acyl-CoA ligand. Simulated annealing omit maps contained clear density for a CoA ligand (Supplementary Fig. 3c). Mass spectrometry analysis confirmed the identity of the ligand as hydrolyzed CoA (Supplementary Fig. 3a,b). Thus, p300\_core copurified from insect cells with endogenous CoA but not with acetyl-CoA or other acyl-CoA variants. To understand how other acyl-CoA variants are accommodated, we crystallized p300 with propionyl-, butyryl- and crotonyl-CoA. Omit maps calculated in the absence of acyl-CoA clearly confirm the position of the ligands reported here (Fig. 2c–e) and of lysyl-CoA and acetyl-CoA reported previously (Fig. 2f,g)<sup>38–40</sup>. Previous structures containing the lysyl-CoA bisubstrate inhibitor show that the substrate lysine invades the active site through a hydrophobic tunnel comprised of Tyr1397, Trp1436, Tyr1446 and Cys1438 that interact with the aliphatic portion of the lysine side chain (Fig. 3a). The propionyl-CoA cocrystal structure showed that the aliphatic propionyl moiety is positioned in the lysine substrate-binding tunnel (Fig. 3b). As in the lysyl-CoA inhibitor, the carbonyl oxygen engages in a hydrogen bond with the backbone amide of Leu1398 and the sulfur atom is directed toward Tyr1467, which is proposed to be the general acid that protonate the sulfur after the acyl-transfer reaction<sup>38</sup>. In the butyryl-CoA and crotonyl-CoA structures, the aliphatic acyl chains are similarly positioned in the lysine substrate-binding tunnel (Fig. 3c,d). Because it contains a more rigid *trans*-unsaturated C $\alpha$ -C $\beta$  bond, the crotonyl moiety adopts a more elongated conformation

as compared to the butyryl chain (Fig. 3d). Superposition with lysyl-CoA shows that the configurations of the propionyl, butyryl or crotonyl moieties are mutually exclusive with lysine substrate binding (Fig. 3e).

p300 uses a direct-transfer mechanism in which acyl-CoA binds first to the HAT domain followed by substrate lysine<sup>41</sup>. As the acyl moieties were not in a conformation compatible with substrate binding, we hypothesized that lysine substrate engagement must displace the acyl group from the substrate-binding tunnel to get access to the carbonyl carbon of acyl-CoA. Such a reaction mechanism would require that the displaced acyl chain be accommodated in the enzyme active site. Inspection of the CoA binding pocket shows that the ligand snakes through a narrow tunnel that opens to the substrate-binding site where the lysine moiety of lysyl-CoA binds. This tunnel contains a cavity bound by the hydrophobic residues Ile1395, Leu1398, Leu1418 and Ile1435. In the acetyl-CoA-bound structure, the methyl moiety of the acetyl group is oriented toward this hydrophobic pocket (Fig. 3f)<sup>40</sup>. Reorientation from the inhibitory position in the substrate-binding tunnel into the cavity would require a  $\sim 180^\circ$  rotation of the carbonyl, such that the hydrogen attached to the oxygen atom bonds to a conserved water molecule that is coordinated by the backbone amide of Trp1436 and carbonyl of Ile1395. In this configuration the aliphatic portion of the acyl-CoA ligand would be positioned in the hydrophobic cavity and the carbonyl in an orientation suitable for nucleophilic attack of the deprotonated primary amine of substrate lysine on the scissile bond. A model of this configuration, which likely represents the conformation just before the reaction occurs, is shown in Figure 3g.

### Conservation of the active site and mutagenesis

HATs have been grouped into five different families based on the sequence similarity within the HAT domain<sup>30</sup>. Each family contains a conserved core region including a 3-stranded  $\beta$ -sheet with a parallel  $\alpha$ -helix spanning one side of the sheet (Fig. 4a). This core region makes conserved interactions with the acyl-CoA cofactor. Surrounding the core are  $\alpha$  and  $\beta$  segments that are structurally divergent between different family members. A molecular surface rendering of the acyl-CoA binding pocket of p300 shows a cavity that is in close proximity to the methyl group of acetyl-CoA (Fig. 4a). Analysis of this cavity revealed that it extends into the interior of the protein (Fig. 4b). hGCN5, which has a more restricted acyl-CoA substrate specificity<sup>36</sup>, does not contain such a cavity (Fig. 4c,d). We therefore predicted that p300 accommodates extended acyl-CoA ligands as a result of the presence of this aliphatic pocket in its active site. Structural comparison reveals that a pocket at an equivalent position is used in enzymes that catalyze transfer of longer acyl chains, including *N*-myristoyltransferase (NMT) and *N*-acyl-L-homoserine lactone (acyl-HSL) synthases. NMT, a member of the GCN5 family, catalyzes attachment of myristic acid (*n*-tetradecanoic acid) onto the N terminus of a number of proteins. The myristoyl group of CoA is accommodated in an extended aliphatic back pocket that is located at an equivalent position of the p300 pocket (Fig. 4e,f). Acyl-HSL synthases are structurally related to acetyltransferases and are involved in quorum sensing in Gram-negative bacteria<sup>42,43</sup>. Acyl-HSL synthases produce *N*-acyl-L-homoserine lactones from the substrates *S*-adenosyl-L-methionine (SAM) and acylated acyl carrier protein (acyl-ACP)<sup>43</sup>. The acyl chain, the length of which can vary from C4–C18, is accommodated in an extended aliphatic pocket,

whose size appears to dictate substrate specificity<sup>43</sup>. Structural superposition shows that the extended pocket of Acyl-HSL synthases is at an equivalent position as that predicted to accommodate the acyl-moiety in p300 (Supplementary Fig. 4a,b). The acyl-chain binding pocket of NMT, TofI and EsaI are significantly larger and more extended as compared to p300, presumably explaining why p300 uses short-chain, but not longer, acyl-CoA variants. The small size of the pocket could explain why hydrolysis of crotonyl- and butyryl-CoA is less efficient than that of propionyl- and acetyl-CoA. The lack of such a pocket in other HATs such as hGCN5, TIP60 and MOF likely explains the more restricted acyl-CoA cofactor requirement for these acyltransferases.

The hydrophobic back pocket of p300 is bounded by partially solvent-accessible residues including Met1376, Ile1395, Leu1398, Leu1418 and Ile1435. Ile1395 and Ile1435 are located at the entrance of the pocket and are nearly invariant among HAT enzymes. To assess the relevance of these residues for acyl-chain transfer, we mutated Ile1395 and Ile1435 to methionine. N-terminally hemagglutinin (HA)-tagged p300 variants were transiently expressed in COS cells, and the impact on activity was measured using an immunoprecipitated (IP)-HAT assay<sup>39</sup>. The I1395M, I1435M or the double I1395M/I1435M mutants revealed similar acetylation activity as compared to wild-type p300 on histone H3-H4 substrate, showing that these mutations do not affect the overall structure and acetylation activity (Fig. 5a). We observed, however, that butyrylation activity was increased for either the I1395M or the double mutant I1395M/I1435M but not for I1435M (Fig. 5a). Introduction of a more bulky residue at this position, I1395F, resulted in a p300 variant that retained acetylation activity but showed diminished butyrylation (Fig. 5b). For crotonylation activity, we also observed an increase with the I1395M mutant, while I1395F resulted in decreased signal (Fig. 5b). In contrast, for propionylation, we did not observe strong effects by mutations in the cavity (Fig. 5b). To more quantitatively characterize the impact on histone acylation, we analyzed the acetylation and butyrylation reaction products using a spectral counting method by MS (Fig. 5c,d and Supplementary Note)<sup>44</sup>. MS analysis of the acetylation reaction revealed that the I1395M mutant showed decreased acetylation at all positions except H4K12 (Fig. 5c). In contrast, we observed a modest increase for histone H3 and H4 butyrylation in the samples treated with p300 I1395M (Fig. 5c,d). Although at several lysine sites only a modest increase was observed, the cumulative effect of these modified lysines could increase the binding affinity of pan-specific anti-butyryl-lysine antibodies and possibly explain the increased signal in the western blot. Together these results indicate that Ile1395 plays a potential role as a 'gatekeeper' residue that controls access of longer acyl-CoA variants into the hydrophobic back pocket of p300. A more flexible Met amino acid residue at this position results in enhanced butyrylation activity, while a more bulky and rigid Phe residue interferes with butyrylation activity, presumably by restricting access of the longer acyl-CoA variants to this back pocket.

### Proposed reaction mechanism

Extensive structural, biochemical, mutational and enzymatic analyses have provided insights into the catalytic mechanism of p300 (refs. 38,41,45). p300 utilizes a "Theorell-Chance" mechanism, a special type of sequential mechanism in which the ternary complex between enzyme, acetyl-CoA and substrate is short lived. The sequential reaction mechanism is

ordered such that acetyl-CoA binds first to p300 before histone substrates bind. Two highly conserved residues, Tyr1467 and Trp1436, play key roles: Tyr1467 acts as a general acid and Trp1436 helps orient the target lysine residue of the protein substrate into the active site<sup>38</sup>. While there is no clear general base for catalysis, recent simulations suggest that Tyr1394 and Asp1507 are involved in a proton-transfer reaction that allows deprotonation of the target substrate lysine<sup>46</sup>. Acetyl-CoA is bound in a conformation that allows direct nucleophilic attack on the carbonyl carbon. However, the aliphatic portions of the longer acyl-CoA variants are accommodated in the substrate-binding tunnel in a conformation that is incompatible with acyl-chain transfer (Supplementary Fig. 5a). We propose that substrate engagement results in displacement of the acyl chain into the hydrophobic cavity made up of Met1376, Ile1395, Leu1398, Leu1418 and Ile1435, and positioning of the lysine amide near the carbonyl carbon atom (Supplementary Fig. 5b). The deprotonated lysine  $-NH_2$  is predicted to attack the carbonyl carbon of acyl-CoA, while Y1467 acts as a general acid to protonate the thiolate anion of CoA (Supplementary Fig. 5c). In the final reaction, the tetrahedral intermediate is resolved and the acyllysine-containing product leaves, followed by CoASH (Supplementary Fig. 5d). Presumably because of the requirement of substrate-assisted rearrangement of the acyl-CoA chain and the restricted size of the back pocket, the rate of transfer catalyzed by p300 is more efficient with short acyl-CoA chains.

## Discussion

Products of cellular metabolism are frequently essential cofactors for chromatin-modifying enzymes, and emerging evidence suggests that metabolism can directly influence chromatin modification and gene expression. Recently, a variety of chemically different lysine acylations, derived from their respective acyl-CoA metabolites, have been identified in chromatin<sup>47</sup>. Because of the presence of a reactive thioester group, acyl-CoA metabolites are intrinsically reactive, and therefore one major question that arises is whether the observed lysine acylations arise non-enzymatically or if there are dedicated enzymes that catalyze their incorporation into chromatin. We have sought to address this issue by studying p300, a well-known histone acetyltransferase, which has been shown to utilize a number of chemically diverse acyl-CoA cofactors to modify histone lysine residues. In addition to lysine acetylation, p300 catalyzes lysine propionylation, crotonylation, butyrylation and, as we show here,  $\beta$ -hydroxybutyrylation<sup>5,24,32</sup>. Like acetylation, crotonylation, butyrylation and  $\beta$ -hydroxybutyrylation are enriched on active gene promoters, thus suggesting that differential histone acylation functionally connects acyl-CoA metabolism and transcriptional regulation<sup>14,19,32</sup>.

We have determined crystal structures of p300 bound to propionyl-CoA, crotonyl-CoA and butyryl-CoA, and we have shown that the extended aliphatic chains are accommodated in the substrate-binding tunnel in a conformation that is incompatible with lysine substrate binding. While it has been clearly established that p300 can catalyze lysine crotonylation and butyrylation, we have now shown that p300 distinguishes between the different acyl-CoA molecules and that the enzymes' reactivity gets weaker with increasing acyl-chain length. We propose that the decrease in catalytic efficiency is due to a substrate-assisted rearrangement of the acyl-CoA chain and to the restricted size of an aliphatic back pocket, which we predict to transiently accommodate the rearranged acyl chain. In agreement with

this model, replacement of I1395 in the back pocket with a more flexible Met residue led to a gain-of-function phenotype, while introduction of a more bulky and rigid Phe residue resulted in a loss-of-function phenotype for butyryl-CoA. Structural analysis of hGCN5 shows that, like p300, the butyryl-CoA C3 and C4 carbons occupy the lysine substrate-binding tunnel<sup>36</sup>. However, hGCN5 does not have an extended aliphatic back pocket to accommodate the acyl chain, and thus for hGCN5 butyryl-CoA is a competitive inhibitor<sup>36</sup>. Other HATs, such as hMOF and hTIP60, also lack a more extended back pocket, which presumably explains why these enzymes are more restrictive with regards to acyl-chain length. Notably, mutations designed to increase the size of the back pocket in hGcn5 and hMOF also allow these enzymes to accommodate larger size acyl groups<sup>48</sup>.

As shown previously, the concentration of cellular crotonyl-CoA influences transcriptional regulation by modulating differential p300-mediated acylation<sup>32</sup>. In such cell culture experiments, acetyl-CoA can be ~1,000-fold more abundant than crotonyl-CoA, and it remains unclear if the physiological concentrations of different acyl-CoA variants are as dynamic<sup>32</sup>. So far few studies have attempted to quantify the relative abundance of different acyl-CoA variants *in vivo*. Measurement of the different acyl-CoAs in the livers of fasting rats showed a relative molar ratio of 40:23:10:1 of acetyl-, propionyl-, butyryl- and crotonyl-CoA<sup>49</sup>. Other measurements have shown a molar ratio of 9:1 and 20:1 of acetyl- and propionyl-CoA in the livers of normal and fastened rats, respectively<sup>50</sup>. Together, these data show consistently higher acetyl-CoA levels under different metabolic regimes. Combined with the lower rate of hydrolysis of the longer acyl-CoA variants by p300, this likely explains why acetylation in chromatin is more abundant as compared to other acylations. However, it is possible that the longer histone acylations are enriched on sites of high histone acylation turnover, such as gene transcriptional start sites (TSSs), and thus compete with histone acetylation<sup>19,32</sup>. We also consider the possibility that other classes of enzymes with more efficient longer-chain acyl transferase activity are involved in these TSS histone acylations.

## Online Methods

### Constructs

The p300\_core sequence encoding residues 1048–1664 was cloned into the RsrII and XhoI sites of pFASTBAC Dual (Invitrogen) vector as a GST-fusion protein with a cleavable tobacco etch virus (TEV) sequence. The sequence contained a Y1467F mutation and a flexible SGGSG amino acid linker replacing the region 1520–1581. A cDNA encoding residues 38–389 of human *SIRT2* was cloned into the NotI and NcoI sites of the pFASTBAC Dual\_p300 vector to obtain the coexpression vector. FLAG-tagged p300s encoding residues 324–2094 was cloned into the RsrII and HindIII sites of pFASTBAC1. Point mutations were introduced by QuikChange mutagenesis (Agilent) and all constructs confirmed by DNA sequencing. p300s was found to contain a T1935A mutation, which was already present in the PCR template.

## Expression and purification

Baculoviruses were maintained in Sf21 insect cells with Sf-900 III SFM medium (Invitrogen). Deacetylated p300 'core' was produced in Hi5 (Invitrogen) insect cells in Express Five SFM medium as described previously<sup>39</sup>. FLAG-tagged human p300 (324–2094) was purified as shown previously<sup>19</sup>.

## Histone acylation assays

Recombinant histones were purified and refolded according to standard procedures<sup>51</sup>. Standard reactions, with 1 µg purified p300, were performed in reaction buffer (25 mM Tris-HCl pH 8, 100 mM NaCl, 1 mM DTT, 0.1 mM EDTA, 10% Glycerol, 1× Complete EDTA-free protease inhibitor; Roche) with 100 ng/mL TSA, 2 µg of purified H3-H4 and 50 µM acyl-CoA. Reactions were incubated in the presence or absence of purified p300 over 1 h at 30 °C. Background non-enzymatic histone acylation was determined under identical conditions, but p300 was omitted from the reaction. Reactions were stopped by addition of SDS-PAGE loading buffer followed by immunoblotting. Alternatively, reaction kinetics were measured by using the DTNB assay. Previous data indicate a  $K_m$  of ~1.2 µM for acetyl-CoA and ~1–10 µM for histone peptides<sup>41</sup>. We chose saturating conditions for both acyl-CoA (250 µM) and H3 (20-mer) histone substrate peptide (100 µM) assuming that the  $K_m$  for acyl-CoA and histone substrate binding are not significantly altered in reactions containing longer acyl-CoA variants. 0.2 µM of p300s was incubated in 180 µl of 100 mM sodium phosphate pH 6.8, 300 mM NaCl, 5 µM zinc chloride with acyl-CoA variants and H3 histone substrate peptide. In agreement with previously published data, HAT activity was in the linear range for 30 min at 30 °C and the acetyl-CoA concentration was saturating. The reaction was stopped by addition of 30 µl quench buffer (6 M guanidinium hydrochloride, 100 mM sodium phosphate dibasic, pH 6.8). To measure CoASH production, 30 µl of 6 mM DTNB in 100 mM sodium phosphate, pH 6.8 and 10 mM EDTA were added and the absorbance at 412 nm recorded. Assays were repeated three times. Background absorbance was subtracted from the absorbance determined for individual reactions. CoASH concentrations were obtained from a standard curve using serial dilutions of CoASH (Sigma). The different acyl-CoAs used were acetyl-CoA (Sigma; A2056), propionyl-CoA (Sigma; P5397), crotonyl-CoA (Sigma; 28007), and butyryl-CoA (Sigma; 20785).

## Mammalian cell culture

COS7 cells were grown at 37 °C under 5% CO<sub>2</sub> atmosphere in DMEM medium supplemented with 10% FBS, 2% Glutamine and 1% Penicillin-Streptomycin (Invitrogen). Cells were grown to ~60–70% confluence on the day of transfection. Transfections were done with Lipofectamine 2000 (Invitrogen) using 1 µl of Lipofectamine for 1 µg vector. Cells were treated with 100 ng/ml Trichostatin A (TSA) from SIGMA (T8552) for 3–4 h before harvest.

## Cell extracts, immunoprecipitation and western blots

After 24 h of transfection, COS7 cells were harvested and extracts prepared in LSDB 500 buffer (50 mM HEPES pH 8.0, 3 mM MgCl<sub>2</sub>, 500 mM KCl, 20% Glycerol, 0.1% NP-40, 1 mM DTT, 100 ng/ml TSA, Complete EDTA-free protease inhibitor; Roche). After

centrifugation, the cell extracts were diluted to 250 mM KCl. For immunoprecipitation, cell extracts were incubated with anti-HA Rat monoclonal antibody (Roche, clone 3F10) for 2 h at 4 °C with rotation and then incubated with magnetic protein G beads (Invitrogen) overnight at 4 °C. After a thorough wash with LSDB 250 mM buffer (50 mM HEPES pH 8, 3 mM MgCl<sub>2</sub>, 250 mM KCl, 20% Glycerol, 0.1% NP-40, 1mM DTT, 100 ng/ml TSA, Complete EDTA-free protease inhibitor; Roche), beads were used for HAT assays. For immunoblotting, proteins were run on a 4–12% Bis–Tris SDS–PAGE (NuPAGE Precast gel, Invitrogen) followed by transfer onto a nitrocellulose membrane (Hybond C+, GE). Membranes were blocked with 5% skim milk in PBST (PBS, 0.1% Tween-20) or 3% BSA in TBST buffer (TBS: Tris base, NaCl pH 7.6, 0.1% Tween-20) then probed with an anti-K-Ac (lysine acetylation) rabbit polyclonal antibody (Cell Signaling; #9441), anti-HA mouse monoclonal antibody (Covance; MMS101R), anti-pan-K-bu (lysine butyrylation; PTM BioLabs), anti-pan-K-cr (lysine crotonylation; PTM Biolabs) or anti-pan-K-pr (lysine propionylation PTM Biolabs), respectively. All antibody dilutions were done as recommended by the manufacturers. Membranes were washed in PBST or TBST buffer before and after incubation with anti-rabbit or anti mouse HRP-conjugated secondary antibody (GE Healthcare; NA934 or NA931), and protein bands were visualized on film after the ECL reaction (GE Healthcare).

### Kac/Kbu quantification

Histones were cut from the gel and washed with 50% ethanol (overnight) followed by water (20 min, twice). After washing, the gel bands were cut into small pieces and dehydrated by acetonitrile for 5 min. Then the gel pieces were washed twice with 100 mM NH<sub>4</sub>HCO<sub>3</sub> and dehydrated by acetonitrile for 5 min, followed by overnight trypsin (Promega) digestion at 37 °C in 100 mM NH<sub>4</sub>HCO<sub>3</sub> buffer. Tryptic peptides were extracted with 50% acetonitrile/5% TFA, 75% acetonitrile/0.1% TFA, and acetonitrile. The solution was vacuum concentrated and the peptides were resuspended in 0.1% TFA followed by desalting using C18-Ziptips.

Tryptic peptides were loaded onto a custom-made capillary column (10 cm length, 75 µm internal diameter) packed with Jupiter C12 resin (4 µm particle size, 90 Å pore size, Phenomenex Inc.) on a nanoLC-1D plus HPLC system (Eksigent Technologies LLC, Dublin, CA). Peptides were eluted with a gradient of 5% to 90% HPLC buffer B (0.1% formic acid in 90% acetonitrile, v/v) in buffer A (0.1% formic acid in water, v/v) over 76 min at a flow rate of 200 nL/min. The eluted peptides were ionized and introduced into a LTQ-Orbitrap Velos mass spectrometer (Thermo Scientific) using a nano-spray source. Full MS scans were acquired over the range  $m/z$  300–1,800 with a mass resolution of 60,000 at  $m/z$  400. MS/MS was operated with a top-20 data-dependent method. For all experiments, the dynamic exclusion time was set to 5 s. Database searching was performed with Mascot 2.1.0 against the Uniprot *Xenopus* protein database. The search parameters included: protein N-terminal acetylation, methionine oxidation, lysine acetylation, lysine butyrylation, lysine mono-/di-/tri-methylation, and arginine mono-/di-methylation as variable modifications; two max missed cleavage sites; precursor ion mass tolerance 20 p.p.m.; MS/MS tolerance 0.5 Da. All the identified peptides were manually verified.

## Crystallization and structure determination

For crystallization, the deacetylated p300 'core' at 4.5 mg ml<sup>-1</sup> was mixed with a three-fold molar excess of the acyl-CoA as described previously<sup>39</sup>. Crystals in the C222<sub>1</sub> space group were grown by sitting-drop vapor diffusion at 4 °C after mixing equal volumes of protein and crystallization solution containing 100 mM Tris, pH 7.5–8.0, 12–17.5% polyethylene glycol MME (monoethyl ether) 2000. Crystals that contain propionyl-CoA were obtained in the presence of 2% DMSO. Crystals were cryoprotected in 20–25% glycerol and frozen in liquid nitrogen. We collected native diffraction data at the ESRF on beamlines ID29 and ID23-2 under a nitrogen gas stream at 100 K at wavelengths of 0.9763 and 0.8726 Å, respectively. All data were processed with XDS (Supplementary Table 1) and the structures determined by molecular replacement with the model for the p300 core (PDB entry 4BHW). The final models contain residues 1046–1664 with a deletion of residues 1517–1581. Analysis of the refined structure by MolProbity showed that there are no residues in disallowed regions of the Ramachandran plot (Supplementary Table 1).

## Supplementary Material

Refer to Web version on PubMed Central for supplementary material.

## Acknowledgments

We thank the staff of ESRF and EMBL-Grenoble for assistance and support in using beamlines ID29, 23-1 and 23-2 and the HTX facility. We thank L. Signor (IBS, Grenoble) and P. Phapale (EMBL) for MS analysis. This work used the platforms of the Grenoble Instruct centre (ISBG; UMS 3518 CNRS-CEA-UJF-EMBL) with support from FRISBI (ANR-10-INSB-05-02) and GRAL (ANR-10-LABX-49-01) within the Grenoble Partnership for Structural Biology (PSB). Z.K. was supported by a fellowship from the EMBL Interdisciplinary Postdoc Programme under Marie Skłodowska-Curie actions Cofund (grant agreement number 291772). This work was supported by the ANR Grant Episperm3 (ANR-15-CE12-0005-02) to S. Khochbin and D.P. and the Worldwide Cancer Research foundation (grant #16-0280) to D.P. Work in S. Khochbin's laboratory is supported by INCa, Fondation pour la Recherche Médicale and Fondation ARC. Work in Y.Z.'s laboratory is supported by NIH grants GM105933, DK107868 and GM115961.

## References

1. Janke R, Dodson AE, Rine J. Metabolism and epigenetics. *Annu Rev Cell Dev Biol.* 2015; 31:473–496. [PubMed: 26359776]
2. Roth SY, Denu JM, Allis CD. Histone acetyltransferases. *Annu Rev Biochem.* 2001; 70:81–120. [PubMed: 11395403]
3. Dhalluin C, et al. Structure and ligand of a histone acetyltransferase bromodomain. *Nature.* 1999; 399:491–496. [PubMed: 10365964]
4. Strahl BD, Allis CD. The language of covalent histone modifications. *Nature.* 2000; 403:41–45. [PubMed: 10638745]
5. Chen Y, et al. Lysine propionylation and butyrylation are novel posttranslational modifications in histones. *Mol Cell Proteomics.* 2007; 6:812–819. [PubMed: 17267393]
6. Tan M, et al. Identification of 67 histone marks and histone lysine crotonylation as a new type of histone modification. *Cell.* 2011; 146:1016–1028. [PubMed: 21925322]
7. Yang YY, Grammel M, Hang HC. Identification of lysine acetyltransferase p300 substrates using 4-pentynoyl-coenzyme A and bioorthogonal proteomics. *Bioorg Med Chem Lett.* 2011; 21:4976–4979. [PubMed: 21669532]
8. Xie Z, et al. Lysine succinylation and lysine malonylation in histones. *Mol Cell Proteomics.* 2012; 11:100–107. [PubMed: 22389435]

9. Dai L, et al. Lysine 2-hydroxyisobutyrylation is a widely distributed active histone mark. *Nat Chem Biol.* 2014; 10:365–370. [PubMed: 24681537]
10. Tan M, et al. Lysine glutarylation is a protein posttranslational modification regulated by SIRT5. *Cell Metab.* 2014; 19:605–617. [PubMed: 24703693]
11. Zhang Z, et al. Identification of lysine succinylation as a new posttranslational modification. *Nat Chem Biol.* 2011; 7:58–63. [PubMed: 21151122]
12. Peng C, et al. The first identification of lysine malonylation substrates and its regulatory enzyme. *Mol Cell Proteomics.* 2011; 10doi: 10.1074/mcp.M111.012658
13. Moellering RE, Cravatt BF. Functional lysine modification by an intrinsically reactive primary glycolytic metabolite. *Science.* 2013; 341:549–553. [PubMed: 23908237]
14. Xie Z, et al. Metabolic regulation of gene expression by histone lysine  $\beta$ -hydroxybutyrylation. *Mol Cell.* 2016; 62:194–206. [PubMed: 27105115]
15. Huang H, Lin S, Garcia BA, Zhao Y. Quantitative proteomic analysis of histone modifications. *Chem Rev.* 2015; 115:2376–2418. [PubMed: 25688442]
16. Cai L, Sutter BM, Li B, Tu BP. Acetyl-CoA induces cell growth and proliferation by promoting the acetylation of histones at growth genes. *Mol Cell.* 2011; 42:426–437. [PubMed: 21596309]
17. Lin H, Su X, He B. Protein lysine acylation and cysteine succination by intermediates of energy metabolism. *ACS Chem Biol.* 2012; 7:947–960. [PubMed: 22571489]
18. Flynn EM, et al. A subset of human bromodomains recognizes butyryllysine and crotonyllysine histone peptide modifications. *Structure.* 2015; 23:1801–1814. [PubMed: 26365797]
19. Goudarzi A, et al. Dynamic competing histone H4 K5K8 acetylation and butyrylation are hallmarks of highly active gene promoters. *Mol Cell.* 2016; 62:169–180. [PubMed: 27105113]
20. Andrews FH, et al. The Taf14 YEATS domain is a reader of histone crotonylation. *Nat Chem Biol.* 2016; 12:396–398. [PubMed: 27089029]
21. Li Y, et al. Molecular coupling of histone crotonylation and active transcription by AF9 YEATS domain. *Mol Cell.* 2016; 62:181–193. [PubMed: 27105114]
22. Du J, et al. Sirt5 is a NAD-dependent protein lysine demalonylase and desuccinylase. *Science.* 2011; 334:806–809. [PubMed: 22076378]
23. Park J, et al. SIRT5-mediated lysine desuccinylation impacts diverse metabolic pathways. *Mol Cell.* 2013; 50:919–930. [PubMed: 23806337]
24. Cheng Z, et al. Molecular characterization of propionyllysines in non-histone proteins. *Mol Cell Proteomics.* 2009; 8:45–52. [PubMed: 18753126]
25. Feldman JL, Baeza J, Denu JM. Activation of the protein deacetylase SIRT6 by long-chain fatty acids and widespread deacylation by mammalian sirtuins. *J Biol Chem.* 2013; 288:31350–31356. [PubMed: 24052263]
26. Bao X, et al. Identification of ‘erasers’ for lysine crotonylated histone marks using a chemical proteomics approach. *eLife.* 2014; 3
27. Garrity J, Gardner JG, Hawse W, Wolberger C, Escalante-Semerena JC. N-lysine propionylation controls the activity of propionyl-CoA synthetase. *J Biol Chem.* 2007; 282:30239–30245. [PubMed: 17684016]
28. Smith BC, Denu JM. Acetyl-lysine analog peptides as mechanistic probes of protein deacetylases. *J Biol Chem.* 2007; 282:37256–37265. [PubMed: 17951578]
29. Jiang H, et al. SIRT6 regulates TNF- $\alpha$  secretion through hydrolysis of long-chain fatty acyl lysine. *Nature.* 2013; 496:110–113. [PubMed: 23552949]
30. Yuan H, Marmorstein R. Histone acetyltransferases: rising ancient counterparts to protein kinases. *Biopolymers.* 2013; 99:98–111. [PubMed: 23175385]
31. Allis CD, et al. New nomenclature for chromatin-modifying enzymes. *Cell.* 2007; 131:633–636. [PubMed: 18022353]
32. Sabari BR, et al. Intracellular crotonyl-CoA stimulates transcription through p300-catalyzed histone crotonylation. *Mol Cell.* 2015; 58:203–215. [PubMed: 25818647]
33. Hu, A., Britton, LM., Garcia, BA. Investigating the specificity of histone acetyltransferase activity for producing rare modifications on histones using mass spectrometry. The 62nd Annual American

- Society for Mass Spectrometry Conference on Mass Spectrometry and Allied Topics; Baltimore, MD. 2014.
34. Berndsen CE, Albaugh BN, Tan S, Denu JM. Catalytic mechanism of a MYST family histone acetyltransferase. *Biochemistry*. 2007; 46:623–629. [PubMed: 17223684]
  35. Leemhuis H, Packman LC, Nightingale KP, Hollfelder F. The human histone acetyltransferase P/CAF is a promiscuous histone propionyltransferase. *ChemBioChem*. 2008; 9:499–503. [PubMed: 18247445]
  36. Ringel AE, Wolberger C. Structural basis for acyl-group discrimination by human Gcn5L2. *Acta Crystallogr D Struct Biol*. 2016; 72:841–848. [PubMed: 27377381]
  37. Thompson PR, et al. Regulation of the p300 HAT domain via a novel activation loop. *Nat Struct Mol Biol*. 2004; 11:308–315. [PubMed: 15004546]
  38. Liu X, et al. The structural basis of protein acetylation by the p300/CBP transcriptional coactivator. *Nature*. 2008; 451:846–850. [PubMed: 18273021]
  39. Delvecchio M, Gaucher J, Aguilar-Gurrieri C, Ortega E, Panne D. Structure of the p300 catalytic core and implications for chromatin targeting and HAT regulation. *Nat Struct Mol Biol*. 2013; 20:1040–1046. [PubMed: 23934153]
  40. Maksimoska J, Segura-Peña D, Cole PA, Marmorstein R. Structure of the p300 histone acetyltransferase bound to acetyl-coenzyme A and its analogues. *Biochemistry*. 2014; 53:3415–3422. [PubMed: 24819397]
  41. Thompson PR, Kurooka H, Nakatani Y, Cole PA. Transcriptional coactivator protein p300. Kinetic characterization of its histone acetyltransferase activity. *J Biol Chem*. 2001; 276:33721–33729. [PubMed: 11445580]
  42. Gould TA, Schweizer HP, Churchill ME. Structure of the *Pseudomonas aeruginosa* acyl-homoserinelactone synthase LasI. *Mol Microbiol*. 2004; 53:1135–1146. [PubMed: 15306017]
  43. Watson WT, Minogue TD, Val DL, von Bodman SB, Churchill ME. Structural basis and specificity of acyl-homoserine lactone signal production in bacterial quorum sensing. *Mol Cell*. 2002; 9:685–694. [PubMed: 11931774]
  44. Carvalho PC, Hewel J, Barbosa VC, Yates JR III. Identifying differences in protein expression levels by spectral counting and feature selection. *Genet Mol Res*. 2008; 7:342–356. [PubMed: 18551400]
  45. Karukurichi KR, Cole PA. Probing the reaction coordinate of the p300/CBP histone acetyltransferase with bisubstrate analogs. *Bioorg Chem*. 2011; 39:42–47. [PubMed: 21111442]
  46. Zhang X, et al. Catalytic mechanism of histone acetyltransferase p300: from the proton transfer to acetylation reaction. *J Phys Chem B*. 2014; 118:2009–2019. [PubMed: 24521098]
  47. Rousseaux S, Khochbin S. Histone acylation beyond acetylation: a terra incognita in chromatin biology. *Cell J*. 2015; 17:1–6. [PubMed: 25870829]
  48. Yang C, et al. Labeling lysine acetyltransferase substrates with engineered enzymes and functionalized cofactor surrogates. *J Am Chem Soc*. 2013; 135:7791–7794. [PubMed: 23659802]
  49. King MT, Reiss PD. Separation and measurement of short-chain coenzyme-A compounds in rat liver by reversed-phase high-performance liquid chromatography. *Anal Biochem*. 1985; 146:173–179. [PubMed: 3993929]
  50. Hosokawa Y, Shimomura Y, Harris RA, Ozawa T. Determination of short-chain acyl-coenzyme A esters by high-performance liquid chromatography. *Anal Biochem*. 1986; 153:45–49. [PubMed: 3963382]
  51. Luger K, Rechsteiner TJ, Richmond TJ. Preparation of nucleosome core particle from recombinant histones. *Methods Enzymol*. 1999; 304:3–19. [PubMed: 10372352]

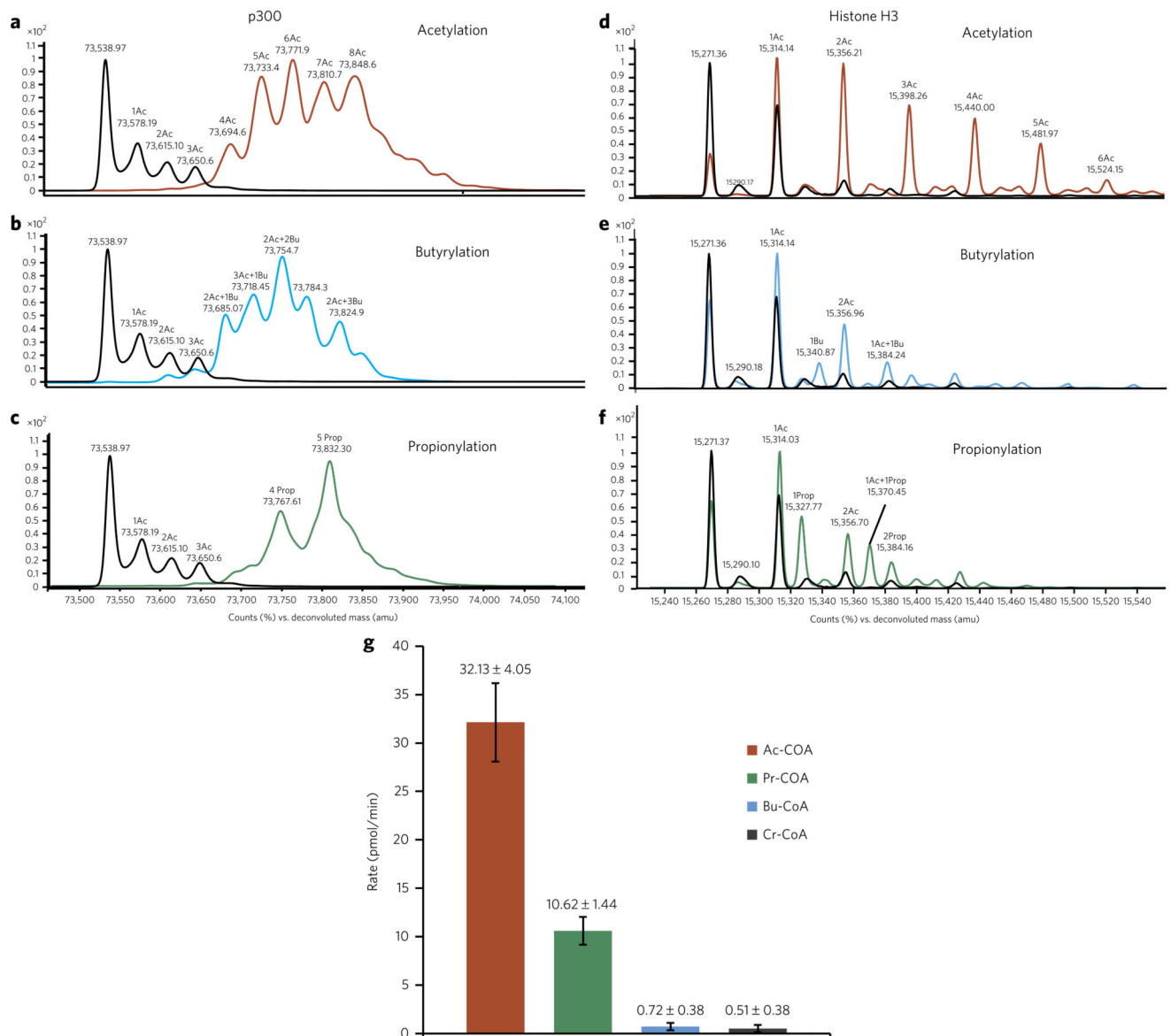


**Figure 1. Acyltransferase activity of p300.**

(a–f) Mass spectrometry analysis using electrospray ionization (ESI) of the p300\_core or histone H3 before (black) and after acylation. Shown are (a) p300 acetylation (red), (b) p300 butyrylation (blue), (c) p300 propionylation (green), (d) H3 acetylation (red), (e) H3 butyrylation (blue), and (f) H3 propionylation (green). The molecular mass (in atomic mass units, amu) and the number of acylation events are indicated. (g) Acyltransferase activity of p300s. The rates of catalysis by p300s were measured using the indicated acyl-CoA cofactors and N-terminal histone H3 peptide. The concentrations of acyl-CoA and substrate peptide H3 (20-mer) were 250  $\mu$ M and 100  $\mu$ M, respectively. p300s was at a concentration of 0.2  $\mu$ M. Experiments were done in triplicate and the error bars represent the s.d.

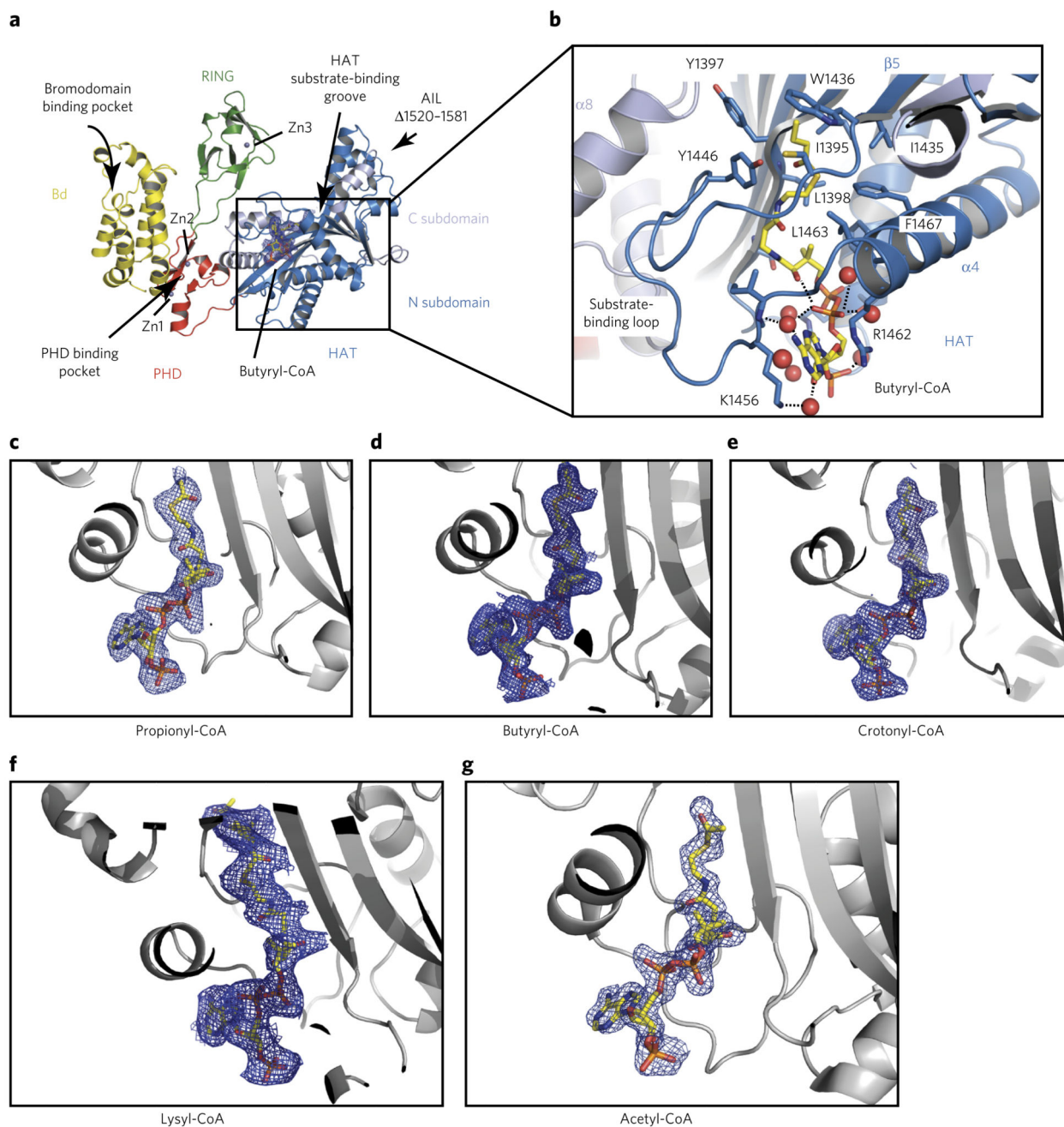


**Figure 2. Structure of p300 in complex with acyl-CoA variants.**

(a) ribbon representations of the p300 core structure. The bromodomain (Bd), RING and PHD domains are shown in yellow, green and red, respectively. The N and C subdomains of the HAT domain are shown in blue and gray, respectively. The position of the deleted autoinhibitory loop (AIL) is indicated with an arrow. Butyryl-CoA is shown in stick representation. (b) The inset displays some of the critical components of the HAT active site: the substrate-binding loop; the proton donor amino acid residue Y1467 (mutated to F in our structure); and amino acid residue W1436, which helps to orient the substrate lysine while

residues K1456 and R1462 are making contact to the adenosine ring of CoA. Amino acid residues in the aliphatic cavity are indicated: I1435, L1398, I1395. **(c–g)** Stick representations of acyl-CoAs and difference density omit maps contoured at  $1.5\sigma$ : **(c)** propionyl-CoA, **(d)** butyryl-CoA, **(e)** crotonyl-CoA, **(f)** lysyl-CoA (PDB code [4BHW](#)), and **(g)** acetyl-CoA (PDB code [4PZS](#)).

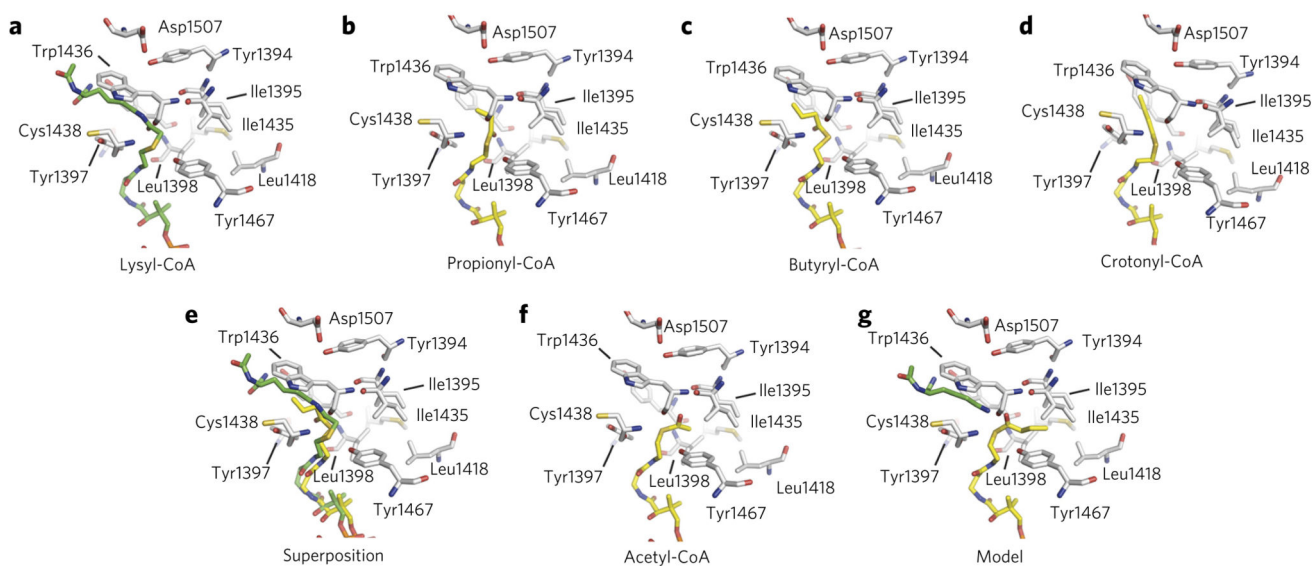


**Figure 3. Comparison of the structure of p30 in complex with different acyl-CoA ligands.** (a) Lysyl-CoA (PDB code 4BHW). (b) Propionyl-CoA. (c) Butyryl-CoA. (d) Crotonyl-CoA. (e) Superposition of lysyl-CoA and butyryl-CoA structures. (f) Acetyl-CoA (PDB code 4PZS). (g) Model of a substrate lysine displacing the butyryl chain into the aliphatic pocket.

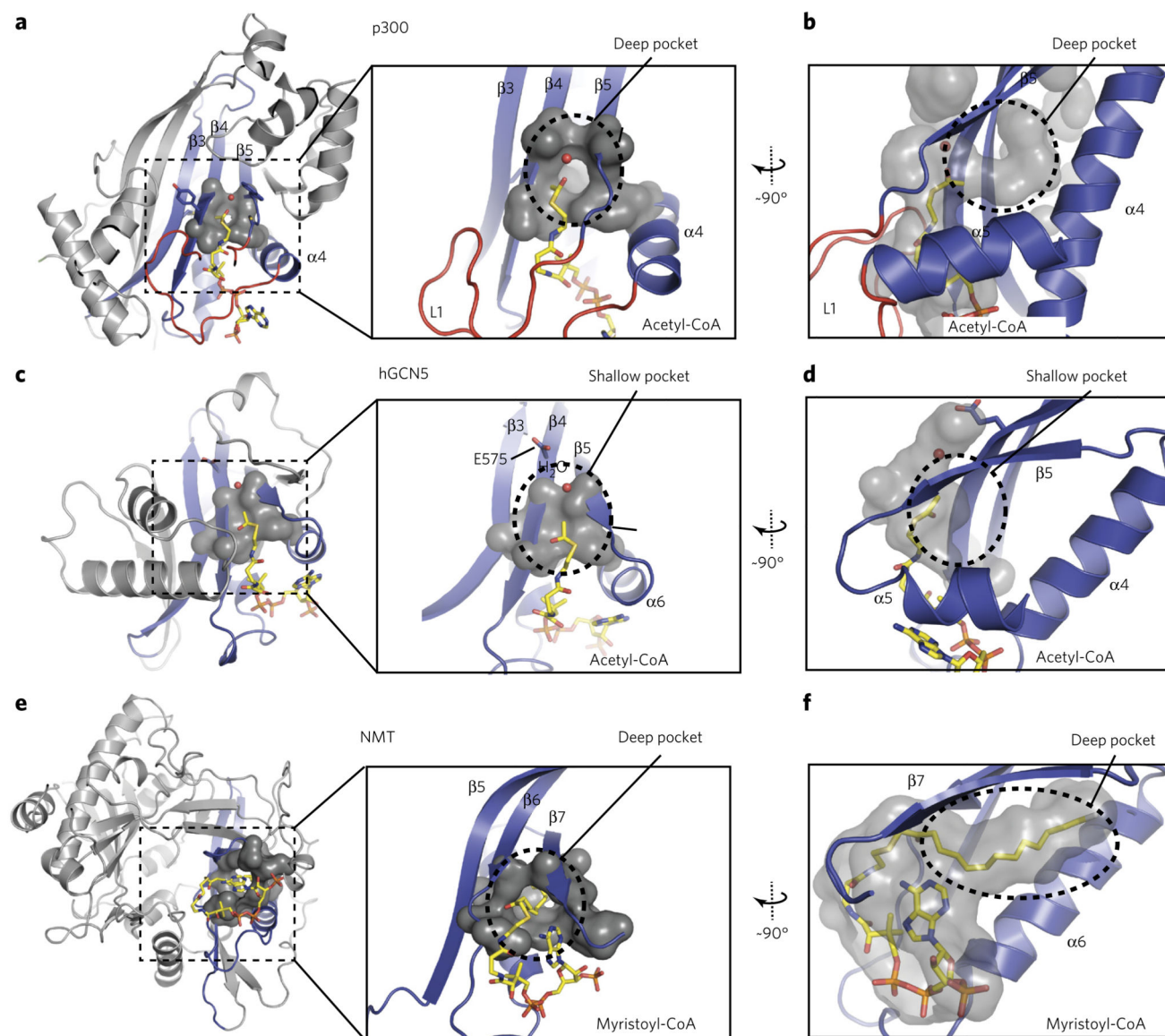


**Figure 4. Comparison of p300 with GNAT acyltransferases.**

The structurally conserved core regions of the HAT domains are colored in blue, and the flanking N- and C-terminal regions in gray. The inset displays the van der Waals surface, colored in gray, around the acetyl group of acetyl-CoA. (a) p300: the non-conserved loop L1 is in red and the cofactor is shown as yellow sticks. (b) The acetyl-CoA binding cavity of p300 is shown as a transparent gray surface. (c) hGCN5 (PDB code [1Z4R](#)). (d) The acetyl-CoA binding cavity of hGCN5 is shown as a transparent gray surface. (e) NMT, *N*-myristoyltransferase (PDB code [1IID](#)). (f) The myristate binding pocket is shown as a transparent surface.

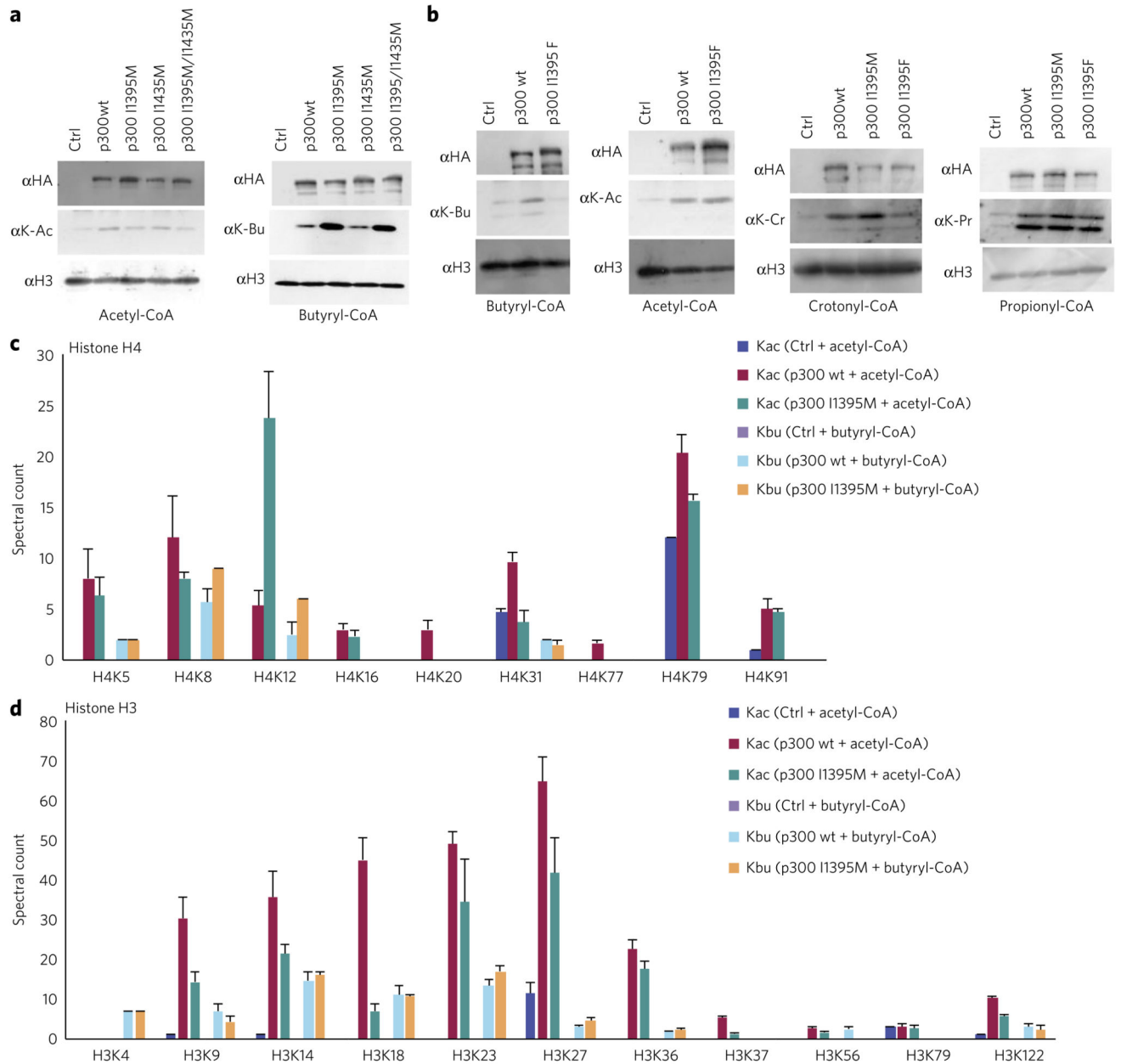


**Figure 5. Analysis of the impact of p300 mutagenesis on the histone acylation profile.**

*In vitro* reconstituted histone H3–H4 tetramers were incubated with the indicated acyl-CoA variants in the presence or absence of the indicated full-length p300 variant. **(a)** Top row, loading control of hemagglutinin (HA)-tagged p300, determined by immunoblotting with anti-HA antibody ( $\alpha$ HA). Middle row, levels of acylation determined by immunoblotting with pan-anti-acetyllysine or pan-anti-butyryllysine antibodies. Bottom row, loading control of histone H3, determined by immunoblotting with anti-H3. Reactions were incubated with acetyl-CoA (left) and butyryl-CoA (right). Ctrl, control in the absence of p300; WT, wild type. Uncropped images are available in Supplementary Figure 6. **(b)** AS in **a**, but for additional p300 mutants and including crotonylation and propionylation. Uncropped images

are available in Supplementary Figure 7. **(c)** The histograms represent the spectral counts of peptides derived from histone H4 from acetylation reactions with p300 wt (red) or mutant I1395M (green). Background acetylation is shown in dark blue. Spectral counts of peptides derived from butyrylation are p300 wt (light blue) or mutant I1395M (orange). Background butyrylation is shown in magenta. The lack of signal indicates that no non-enzymatic butyrylation was detected. **(d)** Acetylated and butyrylated peptides derived from histone H3. Color code is as in **c**. Each sample was analyzed three times and the error bars represent the s.d. of the individual measurements.